



## OPEN ACCESS

## EDITED BY

Burak Tüzün,  
Cumhuriyet University, Turkey

## REVIEWED BY

Xiaoxiao Huang,  
Shenyang Pharmaceutical University,  
China  
Neeraj Kumar,  
Northwestern University, United States  
Mahmoud A. Al-Sha'er,  
Zarqa Private University, Jordan  
Huagang Sheng,  
Shandong University of Traditional  
Chinese Medicine, China

## \*CORRESPONDENCE

Lin-Tao Han,  
✉ hanlintao@hbctm.edu.cn

## SPECIALTY SECTION

This article was submitted to  
Theoretical and Computational  
Chemistry, a section of the journal  
Frontiers in Chemistry

RECEIVED 03 October 2022

ACCEPTED 15 December 2022

PUBLISHED 09 January 2023

## CITATION

Chen P-Y and Han L-T (2023), Study on  
the molecular mechanism of anti-liver  
cancer effect of Evodiae fructus by  
network pharmacology and  
QSAR model.  
*Front. Chem.* 10:1060500.  
doi: 10.3389/fchem.2022.1060500

## COPYRIGHT

© 2023 Chen and Han. This is an open-  
access article distributed under the  
terms of the [Creative Commons  
Attribution License \(CC BY\)](#). The use,  
distribution or reproduction in other  
forums is permitted, provided the  
original author(s) and the copyright  
owner(s) are credited and that the  
original publication in this journal is  
cited, in accordance with accepted  
academic practice. No use, distribution  
or reproduction is permitted which does  
not comply with these terms.

# Study on the molecular mechanism of anti-liver cancer effect of Evodiae fructus by network pharmacology and QSAR model

Peng-Yu Chen<sup>1</sup> and Lin-Tao Han<sup>1,2\*</sup>

<sup>1</sup>Faculty of Pharmacy, Hubei University of Chinese Medicine, Wuhan, China, <sup>2</sup>Key Laboratory of Traditional Chinese Medicine Resources and Prescription, Ministry of Education, Wuhan, China

**Introduction:** Evodiae Fructus (EF) is the dried, near ripe fruit of *Euodia rutaecarpa* (Juss.) Benth in *Rutaceae*. Numerous studies have demonstrated its anti-liver cancer properties. However, the molecular mechanism of Evodiae fructus against liver cancer and its structure-activity connection still require clarification.

**Methods:** We utilized network pharmacology and a QSAR (2- and 3-dimensional) model to study the anti-liver cancer effect of Evodiae fructus. First, by using network pharmacology to screen the active substances and targets of Evodiae fructus, we investigated the signaling pathways involved in the anti-liver cancer actions of Evodiae fructus. The 2D-QSAR pharmacophore model was then used to predict the pIC<sub>50</sub> values of compounds. The hiphop method was used to create an ideal 3D-QSAR pharmacophore model for the prediction of Evodiae fructus compounds. Finally, molecular docking was used to validate the rationality of the pharmacophore, and molecular dynamics was used to disclose the stability of the compounds by assessing the trajectories in 10 ns using RMSD, RMSF, Rg, and hydrogen bonding metrics.

**Results:** In total, 27 compounds were acquired from the TCMSP and TCM-ID databases, and 45 intersection targets were compiled using Venn diagrams. Network integration analysis was used in this study to identify SRC as a primary target. Key pathways were discovered by KEGG pathway analysis, including PD-L1 expression and PD-1 checkpoint pathway, EGFR tyrosine kinase inhibitor resistance, and ErbB signaling pathway. Using a 2D-QSAR pharmacophore model and the MLR approach to predict chemical activity, ten highly active compounds were found. Two hydrophobic features and one hydrogen bond acceptor feature in the 3D-QSAR pharmacophore model were validated by

**Abbreviations:** BP, biological processes; CC, cell components; C-T-P, compounds-targets-pathways; EF, Evodiae fructus; GFA, genetic function approximation; GO, gene ontology; HCC, hepatocellular carcinoma; ICCA, intrahepatic cholangiocarcinoma; KEGG, kyoto encyclopedia of genes and genomes; MF, molecular functions; MLR, multiple linear regression; PLS, partial least squares; PPI, protein-protein interaction; QSAR, quantitative structure activity relationship; TCM, traditional Chinese medicine.

training set chemicals. The results of molecular docking revealed that 10 active compounds had better docking scores with SRC and were linked to residues *via* hydrogen and hydrophobic bonds. Molecular dynamics was used to show the structural stability of obacunone, beta-sitosterol, and sitosterol.

**Conclusion:** Pharmacophore 01 has high selectivity and the ability to distinguish active and inactive compounds, which is the optimal model for this study. Obacunone has the optimal binding ability with SRC. The pharmacophore model proposed in this study provides theoretical support for further screening effective anti-cancer Chinese herbal compounds and optimizing the compound structure.

#### KEYWORDS

Euodiae fructus, liver cancer, network pharmacology, molecular docking, QSAR model, molecular dynamics simulation

## 1 Introduction

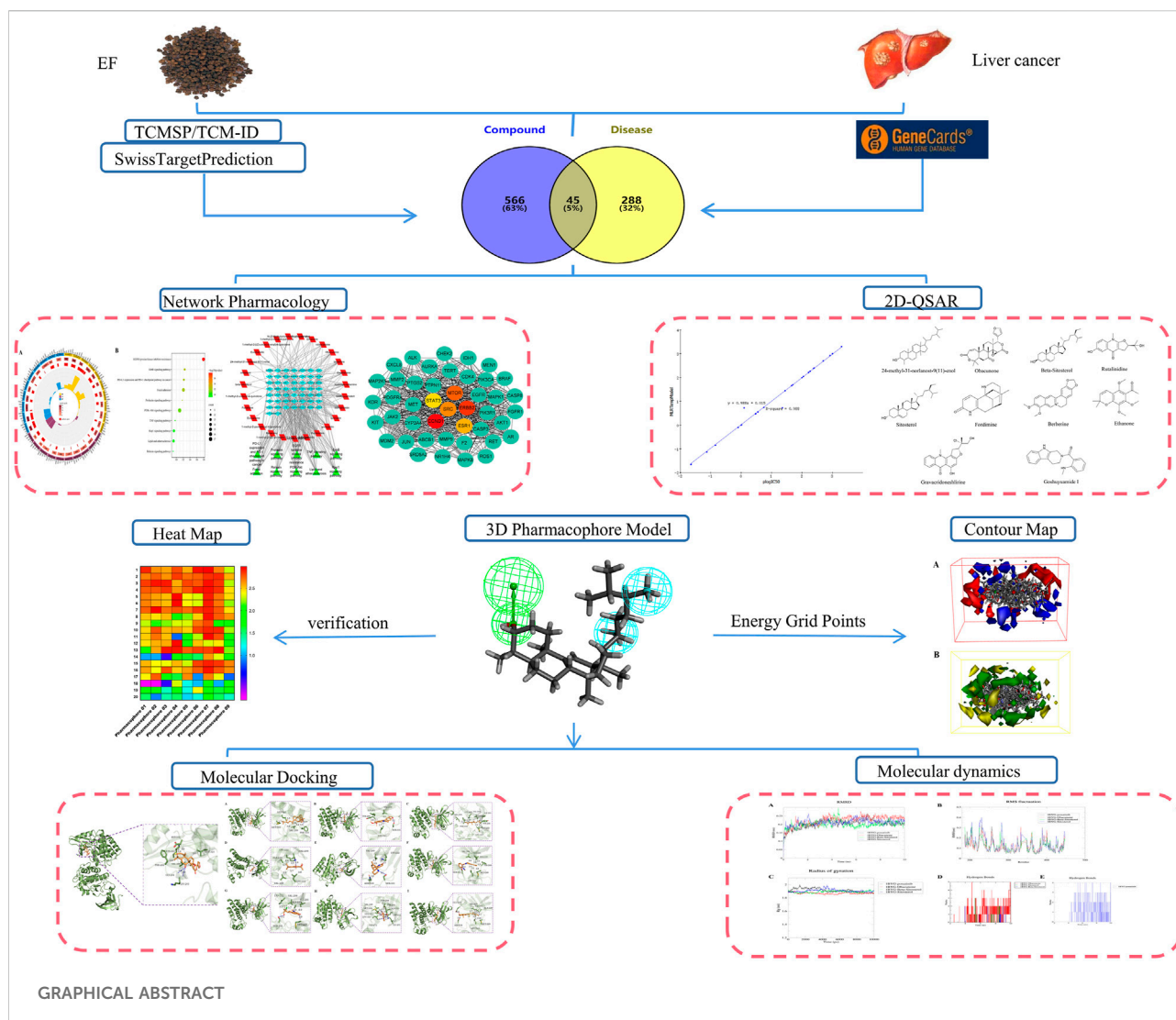
Liver cancer, including intrahepatic cholangiocarcinoma (ICCA) and hepatocellular carcinoma (HCC), is the second-largest cause of cancer-related mortality worldwide and a significant public health issue (Kassebaum et al., 2014). Its incidence rate and mortality have increased annually, and over the past 20 years, it has become the cancer factor in the United States that has caused the biggest increase in mortality (Sia et al., 2017). In 2017, More than half of all liver cancer cases worldwide—5,70,000 new cases—occurred in China. The mortality rate was 26.26/1,00,000, and men had a greater mortality rate than women (37.55/1,00,000 vs. 14.45/1,00,000) (He et al., 2021). Cao et al. (2021) conducted a secondary analysis of cancer statistics from around the world. In 2020, cancer cases in China accounted for 24% of newly confirmed cases worldwide and 30% of cancer deaths worldwide. The death rate from liver cancer rose to second in China in 2020.

Currently, the clinical treatment of liver cancer includes surgery and drug chemotherapy. On the one hand, liver cancer has an extremely dismal prognosis; only 5%–15% of patients are candidates for surgical resection. Therefore, it is only appropriate for early-stage patients with some liver regeneration potential (Anwanwan et al., 2020). On the other hand, the most widely prescribed medication for individuals with advanced stages is the kinase inhibitor sorafenib. However, less than one-third of patients will be able to fully benefit from the course of their treatment. Sorafenib resistance is visible after use, and problems including toxicity and ineffectiveness can also result from prolonged exposure to chemotherapy medicines (El-Serag et al., 2008). Given the poor prognosis of liver cancer, scientists and physicians have been looking for new treatment options to improve patient survival.

Natural products provide distinct advantages in cancer treatment. Natural plant extracts and natural chemicals, as well as traditional Chinese medicines, have gained a lot of attention in recent years for their high-efficiency and low-toxicity anti-cancer

characteristics (Cho et al., 2015). Evodiae Fructus (EF), a traditional medicinal plant, is the dried and nearly ripe fruit of the *Rutaceae* *Euodia rutaecarpa* (Juss.) Benth. EF contains alkaloids, terpenes, flavonoids, phenolic acids, steroids, and phenylpropanoids (Li and Wang, 2020). Modern pharmacological researches have demonstrated its biological properties, including cardioprotective, antibacterial, anti-inflammatory, and anti-tumor effects (Yoon et al., 2013; Zhao et al., 2019; Shan et al., 2020). According to several research, evodiamine, and rutaecarpine in EF had hepatoprotective properties (Yoon et al., 2013). Meanwhile, evodiamine may induce apoptosis in liver cancer cells *via* the WWOX-dependent pathway, as well as the Akt pathway and others, and then exert antitumor effects (Hu et al., 2017; Yang et al., 2017). Furthermore, EF extracts can prevent the development of a variety of cancers, including colon cancer, cervical cancer, and others (Dong et al., 2010; Park et al., 2017). However, the molecular mechanism of EF against liver cancer is currently understudied.

By combining bioinformatics and network analysis, network pharmacology is particularly well suited for the analysis of complex pharmacological mechanisms of multi-compound (Xia and Tang, 2021). The quantitative structure activity relationship (QSAR) method is widely used to investigate the relationship between the physicochemical properties of chemicals and their biological activities in order to obtain a mathematical statistical model for predicting the activity of target chemicals, with differences in structural properties leading to different bioactivities of compounds as the basic principle (Verma et al., 2010). Recently, it has been fashionable to employ QSAR pharmacophore models to investigate the structure-activity connections of TCM and natural compounds in order to uncover their biological activities (Elekofehinti et al., 2021; Li et al., 2022). It is well known that small molecule drugs frequently bind to macromolecular receptors to perform specific biological functions. Molecular docking methods have been widely used in modern drug design to investigate the conformation of ligands within the



binding sites of macromolecular target proteins and to predict their binding mode and binding capacity (Ferreira et al., 2015).

Nowadays, the molecular docking method is an important technique in the field of computer-assisted drug research, and it has become an increasingly important tool for drug discovery. Molecular docking creates drugs based on receptor characteristics and the mode of interaction between receptors and drugs. It can simulate the interaction of molecules and proteins at the atomic level to elucidate the binding sites and binding characteristics of small molecules on target proteins, as well as the fundamental biochemical processes. Molecular docking can also predict ligand and receptor conformation and calculate parameters such as affinity to evaluate binding. This technique is accurate and low-cost, and it is currently used primarily for drug design and the elucidation of biochemical processes (Meng et al., 2011).

In this study, active compounds and key targets of EF were first screened using the network pharmacology method, followed

by GO and KEGG analysis to investigate the molecular mechanism. The pIC<sub>50</sub> of active compounds in EF were successfully predicted by the 2D-QSAR pharmacophore model, and the hiphop method was used to construct the 3D-QSAR pharmacophore model. Finally, molecular docking was used to confirm the binding modes of ligands to proteins. In the graphic abstract, the main concept under study is displayed.

## 2 Materials and methods

### 2.1 Network pharmacology

#### 2.1.1 Chemical compounds and targets acquisition

We use the Traditional Chinese Medicine Systems Pharmacology Database and Analysis Platform (TCMSP,

<http://tcmssp.com/tcmssp.php>) and the Traditional Chinese Medicine Information Database (TCM-ID, <http://bidd.grouptcmid.com/index.html>) to obtain the chemical compounds in EF. The OB value (Oral bioavailability) and DL value (Drug-likeness) used as a reference for filter chemicals are 30% and .18%, respectively. Their structures were retrieved in SDF format from the PubChem database. Then we utilized the SwissTargetPrediction (<http://www.swisstargetprediction.ch/>) to find compound targets, entered “liver cancer” at GeneCards (<https://www.genecards.org/>) to find genes associated with liver cancer (score > 30), and then we analyzed the intersection targets with the aid of the venny2.1.0 platform to find the appropriate targets of EF against liver cancer.

### 2.1.2 GO/KEGG analysis

DAVID Bioinformatics Resources (<https://david.ncifcrf.gov/home.jsp>) is a well-known bioinformatics resource system for functional annotation and enrichment analysis of gene lists (Sherman et al., 2022). We submitted the intersection targets of EF treatment for liver cancer to the DAVID database, chose *Homo sapiens* as the species, and obtained items from Gene Ontology (GO) and the Kyoto Encyclopedia of Genes and Genomes (KEGG). It is used to annotate biological functions and analyze signal pathways of key targets.

### 2.1.3 C-T-P and PPI network construction

The “Compounds-Targets-Pathways” (C-T-P) network is frequently used to analyze the interactions between compounds, targets, and pathways (Chen et al., 2021). Furthermore, the analysis of Protein-protein Interaction (PPI) networks can contribute to a better understanding of disease molecular mechanisms by systematically analyzing and discovering important targets (O’Reilly et al., 2019). The PPI network was obtained using the STRING database (<https://string-db.org/>). The C-T-P network was built using the Cytoscape 3.9.1 software, and we ranked compounds by degree value to determine their significance. The key targets in the PPI network were examined using Cytoscape 3.9.1’s cytohubba plugin analysis.

## 2.2 Construction of the QSAR model

We obtained 45 SRC inhibitors based on the literature and the Selleck website (<https://www.selleck.cn/>) (Martin et al., 2006; Bain et al., 2007; Schenone et al., 2007; Hiscox and Nicholson, 2008; Fathi et al., 2019; Ma et al., 2020). The 3D structural formulas were downloaded from PubChem, and energy was minimized through batch processing using Discovery Studio Software (Discovery Studio 2019; BIOVIA; San Diego, United States). Using the “Creat Training and Test Data” function module, all SRC inhibitor compounds were randomly divided into a training set (35 compounds) and a test set (ten

compounds) (Supplementary Figures S7, S8). The resulting activity values of the training and test set compounds ranged across four orders of magnitude, ensuring the model’s accuracy. Quantitative structure-activity relationships (QSAR) are a powerful computational method for analyzing data based on chemical structure. The QSAR pharmacophore model was created by establishing a statistical mathematical link between calculated chemical descriptors of molecular structure and experimentally measured values of these molecules’ biological activity, which can be used to predict biological activity with a variety of target chemical products (Muratov et al., 2020).

### 2.2.1 Construction of the 2D-QSAR pharmacophore

In this study, 2D-QSAR models were built by calculating the molecular properties of the training and test sets using Discovery Studio software. The forward selection by partial least squares (PLS) method and the stepwise multiple linear regression (MLR) method validated by the external test set prediction method were used to build the 2D-QSAR model (Hajalsiddig et al., 2020). Furthermore, the genetic function approximation method (GFA) is an intelligent regression algorithm that simulates biological evolution and natural selection in nature. Because GFA provided a better fit to the training set, it was also commonly used for QSAR modeling (Wang et al., 2012). The  $pIC_{50}$  value is typically used to describe the biological activity of a substance, The “calculate molecular properties” module was used to calculate a number of molecular descriptors included AlogP, molecular weight, the total number of bonds, the minimum energy of conformation (kcal/mol), volume, surface area, and other properties (Dwivedi et al., 2011; Imran et al., 2015). Some statistical parameters, such as the coefficient of determination ( $r^2$ ), adjusted  $r^2$  ( $r^2$  adj), and prediction (PRESS)  $r^2$  ( $r^2$  pred), determine the accuracy of our constructed model.

### 2.2.2 Construction of the 3D-QSAR pharmacophore

Similarly, we built 3D-QSAR models with Discovery Studio software, typically using the HipHop method. The hip-hop method uses the three-dimensional structures of a series of known target inhibitors/activators to describe the common features of biological activities, develop pharmacophore models, and finally generate the best quantitative pharmacophore model for 3D querying (Wang et al., 2008). First, we screened 10 compounds with higher EF activities and imported their structures’ SDF format (3D) into Discovery Studio software. The principal value and maximumomifeat value of each compound are then defined. Compounds were designated as active when their  $IC_{50}$  was less than  $1\mu M$ , the Principal value was set to 2, and the Maxomifeat value was set to 0. When their  $IC_{50}$  was greater than  $1\mu M$ , both the Principal and Maxomifeat values were set to 1 (Rampogu et al., 2018).

Feature mapping is used to identify compound feature elements and investigate molecules that contain those main feature elements. Furthermore, we performed pharmacophore feature element selection to select those included in the HypoGen module, which generally included five types of feature elements: hydrophobic, hydrogen bond donor (Donor), hydrogen bond acceptor (Acceptor), positively charged ion center (Ionizable Positive), and aromatic ring center (Ring Aromatic). Next, the Maximum Conformation was set to 255 and the Energy Threshold to 10 (Jiang et al., 2016). Finally, the compounds from the test set were used to validate the pharmacophore model.

The 3D structure of a set of ligands was used to calculate the potential energy in the discovery Studio software's 3D-QSAR method, and the potential energy was then used as a descriptor to build the model. Such a model correlates the molecular field and activity and links the three-dimensional structure and biological activity (Ahmed et al., 2017). The equation is as follows:

$$\text{Activity (Predicted)} = \sum_{i=1}^{N_{EP}} CEP(i)VEP(i) + \sum_{i=1}^{N_{VDW}} CVDW(i)VVDW(i)$$

where,  $N_{EP}$  represents the number of descriptors of electrostatic potential (EP),  $CEP(i)$  is the model coefficient of EP descriptor, and  $VEP(i)$  is the electrostatic potential value on the grid points. Furthermore,  $N_{VDW}$  is the number of descriptors of Van Der Waals (VDW) interactions,  $CVDW(i)$  is the model coefficient of VDW descriptor  $I$ , and  $VVDW$  is the VDW interaction potential energy on the grid points. In summary, the predicted activity of a compound is the linear sum of the model coefficients multiplied by their corresponding grid values.

## 2.3 Molecular docking

Molecular docking is currently a key method in drug design since it enables research of ligand binding modalities, stable ligand receptor complex intermolecular interactions, and binding energy predictions (Huang and Zou, 2010). The top ten active compounds in the pharmacophore model were chosen as ligand molecules, and the key target SRC was chosen as the target protein for AutoDock molecular docking tests. We obtained SRC crystal structure 1BYG from the PDB database. To improve reliability, we chose reference drugs such as Ponatinib and Dasatinib, which are SRC inhibitors that are already in clinical use (Ceppi et al., 2012; Roskoski, 2015). Furthermore, STAUROSPORINE (STU), the original SRC ligand, is used as a control (1BYG).

The SRC protein structure (1BYG) was obtained from the Protein Data Bank (<https://www.rcsb.org/>). First, the proteins were processed with PyMOL software, which removed water molecules and extracted ligands while recording the docking site

coordinates (Getbox plugin) of the chosen ligands. The small molecules were then preprocessed with AutoDockTools1.5.6, and the proteins were hydrogenated and charged. After that, one profile (including protein and ligand structure files as well as docking site information) was created for AutoDock Vina docking. Finally, information about the docking results was obtained from the PLIP website (<https://plip-tool.biotec.tu-dresden.de/plip-web/plip/index>), and the docking results were visualized using PyMOL software.

## 2.4 Molecular dynamics simulation

GROMACS is used for molecular dynamics (MD) simulations of protein-ligand complexes. This experiment included compounds with high docking scores that formed complexes with proteins such as 1BYG-Obacunone, 1BYG-Beta-sitosterol, and 1BYG-Sitosterol. Meanwhile, 1BYG-Ponatinib was used as a control. We used the Acyppe portal and the AMBER force field to generate topology files for the ligands, with SPC as the water model. The relevant scripts were run to add water models, ions, and balance charges. The systems were stabilized by running energy minimization (100 ps) with the steepest descent algorithm. After that, we used the Verlet algorithm for NVT equilibration for 100 ps (2fs steps) and the Berenson algorithm for NPT equilibration for 100 ps (2fs steps) (Adelusi et al., 2021). To ensure that atoms did not jump out of the PBC, the "trjconv" module was used for system processing (periodic boundary conditions). The stability was assessed using root mean square deviation (RMSD), root mean square fluctuation (RMSF), radius of gyration (Rg), and hydrogen bond analysis.

## 3 Results and discussion

### 3.1 Network pharmacology analysis

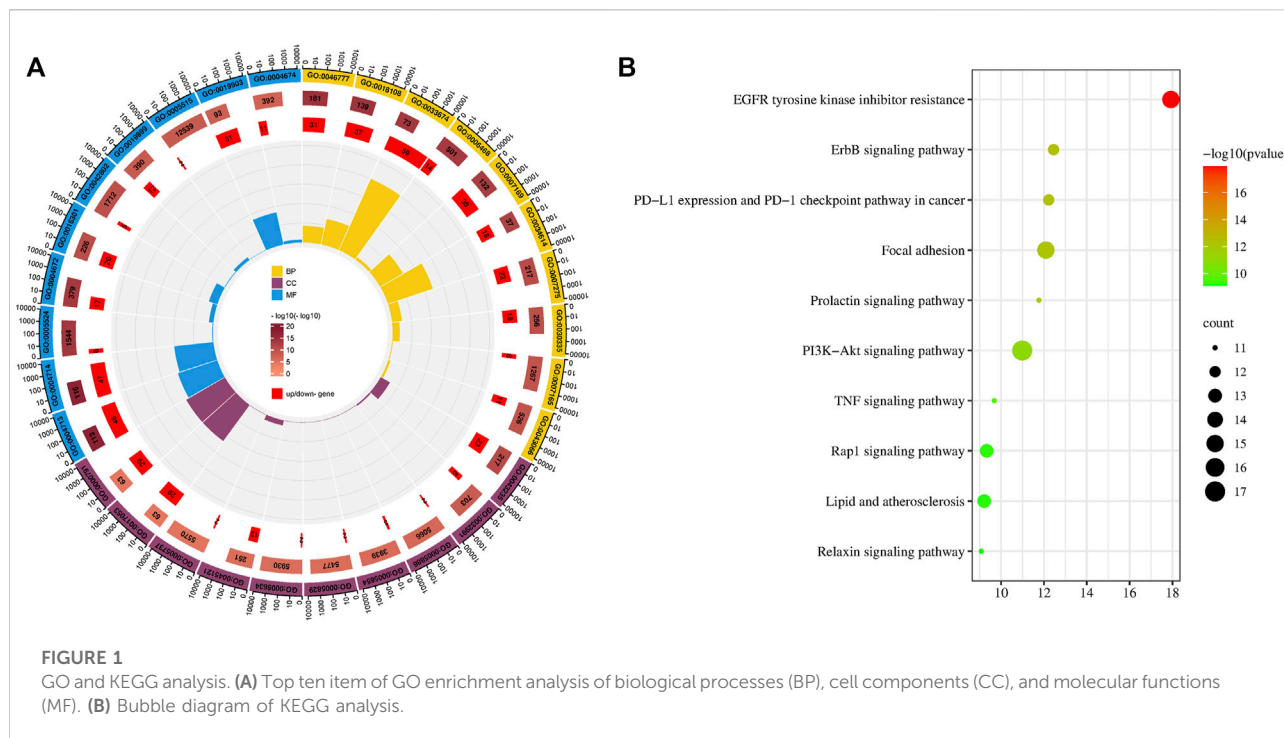
#### 3.1.1 Chemical compounds and targets acquisition

With OB 30% and DL .18 as thresholds, 27 compounds from EF (Supplementary Table S1) were screened from the TCMSP and TCM-ID databases. SwissTargetPrediction identified a total of 611 compound targets. Genecards identified 333 liver cancer targets, and Venn analysis revealed 45 intersecting targets that could be used by EF to play pharmacological roles in the anti-liver cancer process (Supplementary Figure S1; Supplementary Table S2).

#### 3.1.2 GO/KEGG analysis results

We screened the top ten items in the GO and KEGG enrichment analyses in ascending order of  $p$ -value (Figure 1). The results of the Go analysis indicate that the biological





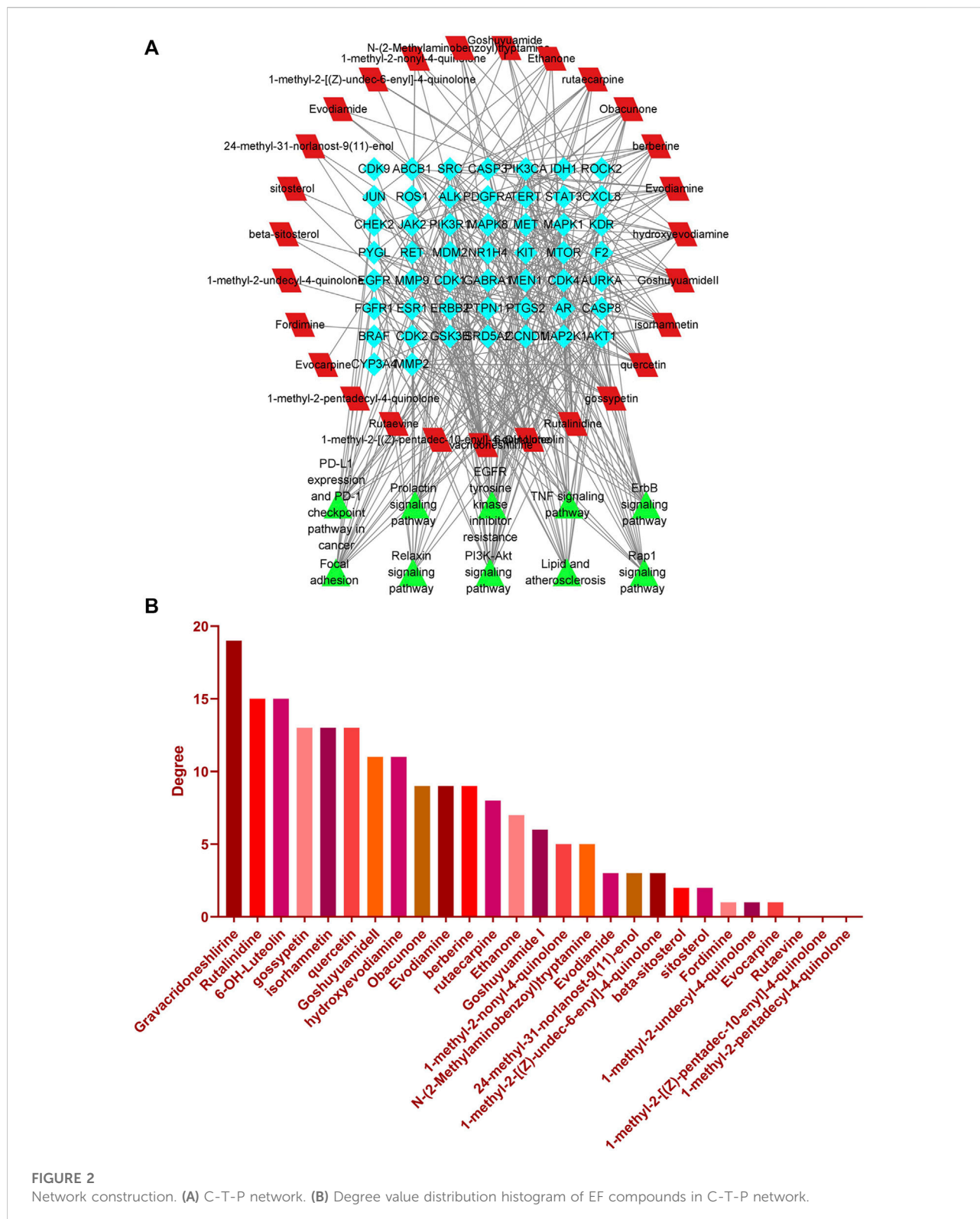
processes (BP) mainly involve the development of multicellular organisms, cellular response to reactive oxygen species, protein autophosphorylation, peptidyl-tyrosine phosphorylation, positive regulation of kinase activity, protein phosphorylation, and transmembrane receptor protein tyrosine kinase signaling pathway. Cell Components (CC) include the receptor complex, the macromolecular complex, the plasma membrane, the nucleoplasm, the cytosol, the nucleus, the membrane raft, the cytoplasm, and so on. Protein tyrosine kinase activity, transmembrane receptor protein tyrosine kinase activity, ATP binding, protein kinase activity, kinase activity, identical protein binding, enzyme binding, protein binding, and so on are examples of Molecular Functions (MF) (Supplementary Table S3).

A total of 138 pathways with significant meaning ( $P < 0.05$ ) were enriched by KEGG analysis. The top ten key pathways include EGFR tyrosine kinase inhibitor resistance, ErbB signaling pathway, PD-L1 expression and PD-1 checkpoint pathway in cancer, Focal adhesion, Prolactin signaling pathway, PI3K-Akt signaling pathway, TNF signaling pathway, Rap1 signaling pathway, Lipid and atherosclerosis, and others. The EGFR and ErbB signaling pathways are the highest ranked in KEGG and are upstream in other pathways. EGFR and ErbB are members of a family of cell membrane protein receptors that can receive stimuli and send signals downstream, triggering a series of regulatory processes for both life activities and diseases. EGFR inhibition has been shown in studies to inhibit HCC cell survival, migration, and invasion (Chen et al., 2019; Jin et al., 2021). The

ErbB-PI3K-AKT pathway can promote the growth and spread of hepatocellular carcinoma (Ni et al., 2020). Overexpression of focal adhesion kinase (FAK) occurs frequently in human HCC tissues, and simultaneous overexpression of FAK increases AR expression, which leads to HCC formation in mice (Shang et al., 2019). Certainly, there is also evidence that the Prolactin signaling pathway, the PI3K-Akt signaling pathway, the TNF signaling pathway, and other pathways play important roles in the process of liver cancer (Dumaual et al., 2012; Meng et al., 2021; Miethe et al., 2021).

### 3.1.3 Network analysis

We can further investigate the relationship between EF compounds, targets, and pathways by building the C-T-P network with Cytoscape 3.9.1. The C-T-P network, as shown in Figure 2A, demonstrates interactions between compounds-targets-pathways. This network contains 314 edges that represent interactions between nodes. The network also included 88 nodes: 27 shared by red square nodes representing compounds, 51 shared by blue diamond nodes representing targets, and 10 shared by green triangle nodes representing signaling pathways. The higher the degree value of the node, the more critical this node is. This network reflects the characteristics of multi-compound and multi-target interactions in TCM. Furthermore, it demonstrated that these chemicals have a better potential for bioactivity against liver cancer. In the C-T-P network, higher degree values for compounds such as gravacridoneshlorine, gossypetin, quercetin, isorhamnetin,



obacunone, and 6-OH-luteolin. It suggests a greater likelihood that they may have potential liver cancer-preventing actions (Figure 2B). Meanwhile, we screened critical targets based on

their degree values (Supplementary Table S4). The results showed that SRC, which was thought to be the crucial target in this investigation, had the greatest degree value.

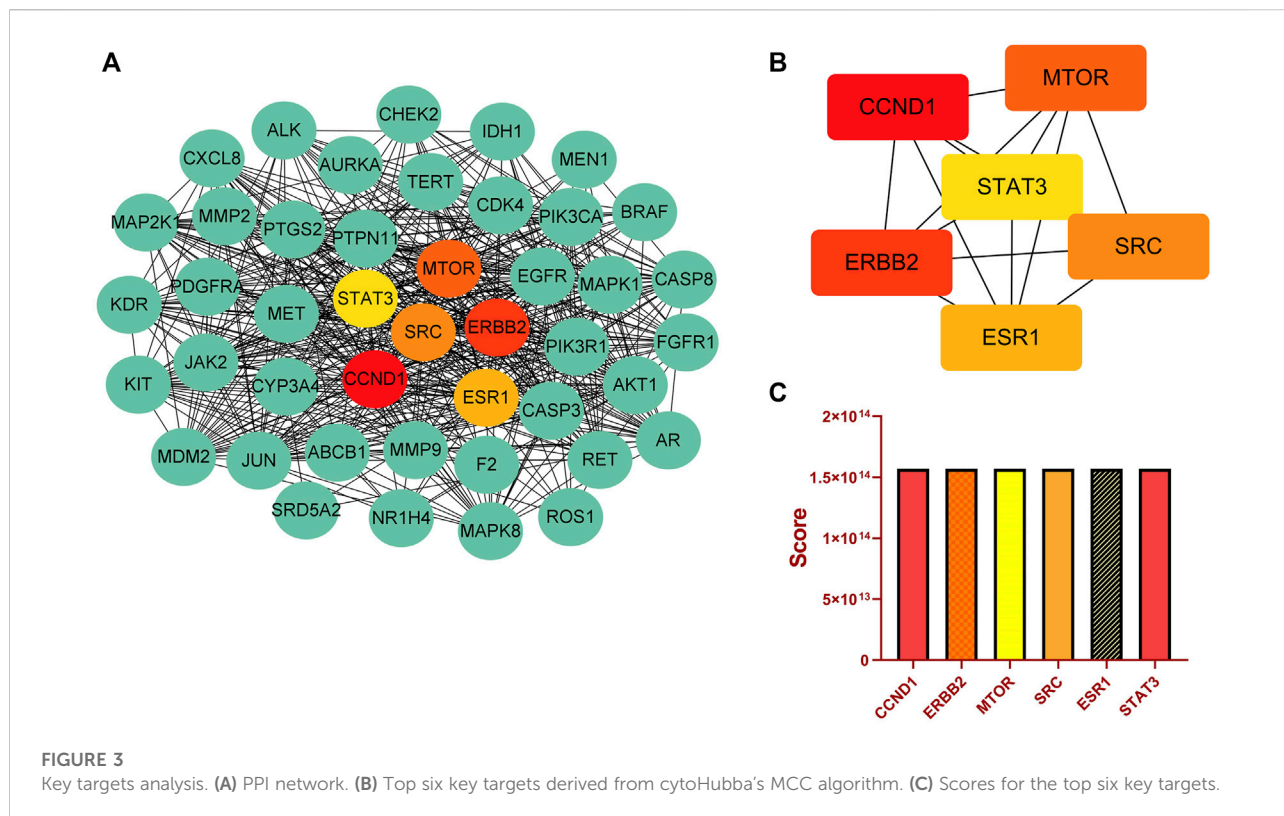


**TABLE 1** Based on the 2D-QSAR test set compound experimental and predicted activity pIC<sub>50</sub> (μM).

Training no.	Experiment pIC <sub>50</sub>	Predicted GFA	Residual <sup>a</sup>	Predicted MLR	Residual <sup>b</sup>	Predicted PLS	Residual <sup>c</sup>
1	1.046	-.676	1.722	.603	.443	3.213	2.167
2	2.699	2.858	.159	1.958	.741	2.661	.038
3	-1.758	-1.285	.474	-1.329	.429	-.898	.861
4	2.301	1.271	1.030	2.049	.252	2.399	.098
5	1.695	.968	.727	1.498	.197	1.082	.613
6	3.000	2.858	.142	3.255	.255	2.187	.813
7	-.146	.662	.808	-.427	.281	.488	.634
8	2.046	1.783	.263	2.543	.497	2.148	.102
9	3.301	4.176	.875	3.365	.064	2.226	1.075
10	.208	.968	.760	.695	.488	.899	.691
r <sup>2</sup>		.9117		.988		.800	
r <sup>2</sup> (adj)		.8928		.981		.787	
r <sup>2</sup> (pred)		.8564		.975			

<sup>a</sup>GFA-Experiment pIC<sub>50</sub>.

<sup>b</sup>MLR-Experiment pIC<sub>50</sub>.

<sup>c</sup>PLS-Experiment pIC<sub>50</sub>.

Moreover, we identified important target proteins in the PPI network using the Cytoscape cytohubba plugin. There are eleven computational methods available to Cytoscape, which

can examine the key nodes in bioinformatic networks. At the moment, MCC is regarded as being the best method (Chin et al., 2014). In addition, The PPI network showed high degree



TABLE 2 The activity pIC<sub>50</sub> (μM) of PD Based on the 2D-QSAR model.

Pubchem CID	Compound	Predicted (MLR) pIC <sub>50</sub>
5319810	1-methyl-2-[(Z)-undec-6-enyl]-4-quinolone	-1.059
13967189	1-methyl-2-nonyl-4-quinolone	-.674
5319811	1-methyl-2-undecyl-4-quinolone	-.880
162926950	24-methyl-31-norlanost-9(11)-enol	1.733
5281642	6-OH-Luteolin	-1.040
12457	Berberine	.318
222284	beta-Sitosterol	1.374
624052	Ethanone	.318
5317303	Evocarpine	-1.266
189454	Evodiamide	.023
442088	Evodiamine	-.056
58757248	Fordimine	.725
5317827	Goshuyamide_I	.142
5317828	GoshuyamideII	-.265
5280647	gossypetin	-1.035
163102888	Gravacridoneshlerine	.151
56967381	hydroxyevodiamine	.005
5281654	Isorhamnetin	-.944
5319506	N-(2-Methylaminobenzoyl)tryptamine	-.393
119041	Obacunone	1.491

values for CCND1, ERBB2, MTOR, SRC, ESR1, and STAT3 (Figures 3A, B). Histograms depict the score values of these targets (Figure 3C; Supplementary Table S5). We discovered that SRC not only plays an important role in the C-T-P network, but also ranks high in the PPI network. SRC has a high score in comparison to the other core proteins in the PPI network, and there are close interactions. Using KEGG analysis, we discovered that SRC is involved in a number of significant signaling pathways. EGFR/ErbB-2 can activate downstream SRC proteins, and SRC can then encourage liver cancer cell growth and metastasis through focal adhesion and the PI3K-Akt signaling pathway (Ren and Schaefer, 2002; You et al., 2018; Mo et al., 2020; Luo et al., 2021). Meanwhile, a large body of literature has reported on the role of SRC in liver cancer and has shown that SRC could be a therapeutic target in liver cancer (Tong et al., 2015; Zhao et al., 2020; Yang et al., 2021). Additionally, Liao et al. (2014) demonstrated through experiments that EF extract might reduce SRC expression to reduce hepatotoxicity. Therefore, we believe SRC was the most important key target in this study.

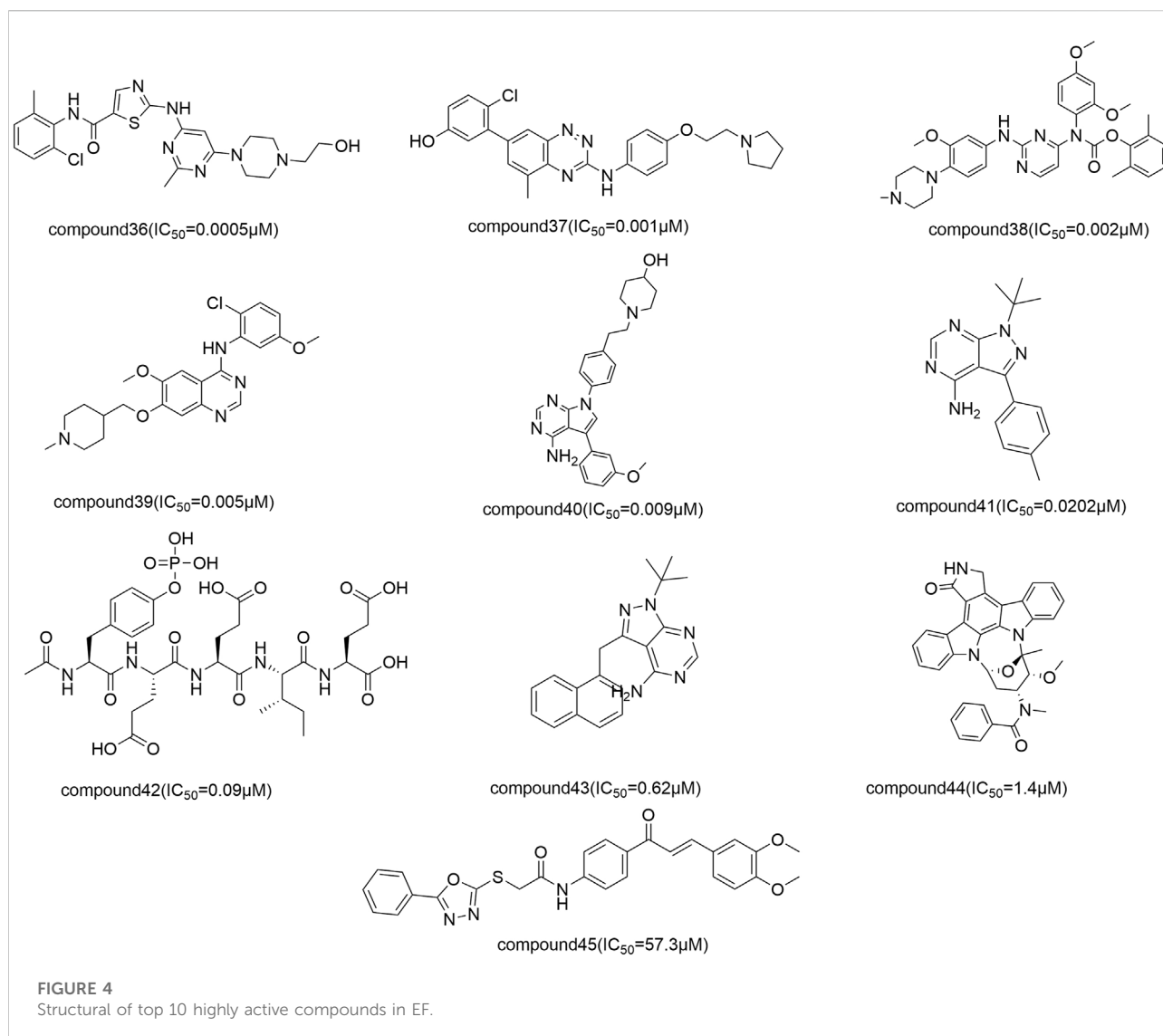
## 3.2 2D-QSAR model analysis

### 3.2.1 Construction of 2D-QSAR pharmacophore model

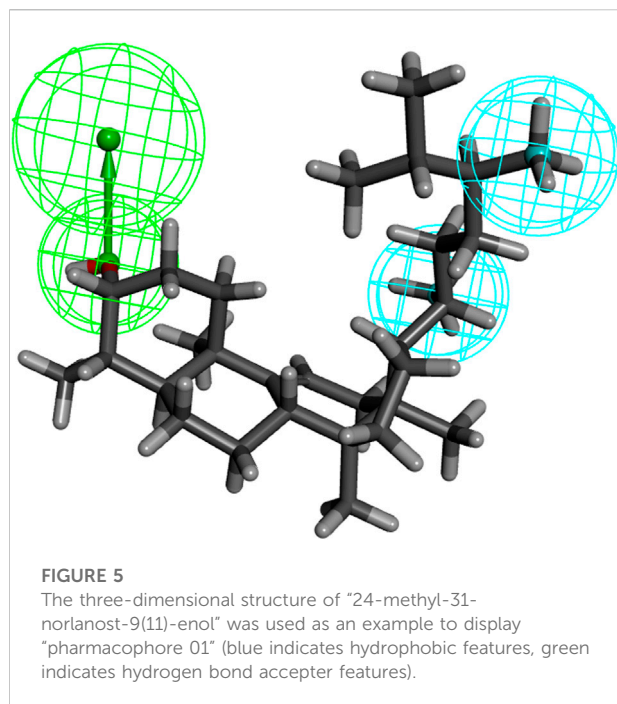
To build the 2D-QSAR model, we used the GFA, MLR, and PLS linear fitting algorithms in the Discovery Studio software. The linear regression equations (Supplementary Figures S3–S5) revealed that the correlation regression coefficients  $r^2$  of the three algorithms (GFA, MLR, and PLS) were .912, .988, and .800, respectively, demonstrating their good predictive ability and prediction accuracy for pharmacophore models, particularly MLR. Then, using these three techniques, we created 2D-QSAR models to forecast the biological activities (pIC<sub>50</sub>) of the compounds in the test set. The results showed that (Table 1) the predicted pIC<sub>50</sub> values of the compounds based on GFA and PLS algorithms showed relatively large deviations from the experimental pIC<sub>50</sub> values, indicating lower accuracy.

### 3.2.2 Prediction of EF activity from 2D-QSAR models

The activity of the EF compounds screened was predicted by our 2D-QSAR model using the MLR method (Table 2). The top highly

**TABLE 3** Common characteristic parameters of active compounds displayed by pharmacophore models.

Pharmacophore	Feature	Rank	Direct hit	Partial hit	Max hit
01	HHA	57.220	1111111111	0000000000	3
02	HHA	57.042	1111111111	0000000000	3
03	HHA	55.151	1111111111	0000000000	3
04	HHA	52.597	1111111111	0000000000	3
05	HHA	49.170	1111111111	0000000000	3
06	HHA	48.528	1111111111	0000000000	3
07	HHA	42.982	1111111111	0000000000	3
08	HHA	41.428	1111111111	0000000000	3
09	HHA	32.624	1111111111	0000000000	3

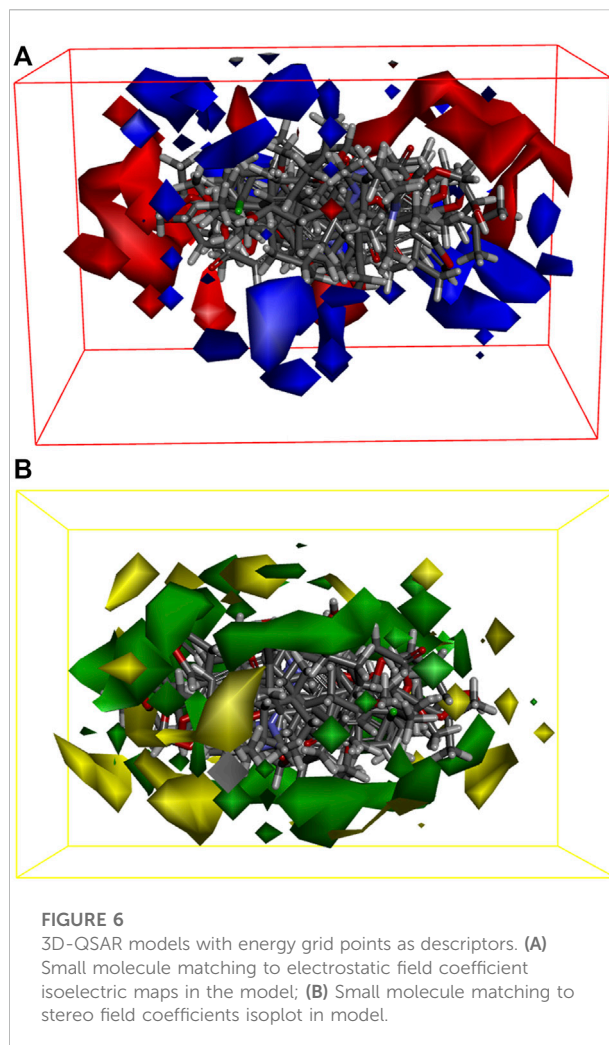


active compounds were 24-methyl-31-norlanost-9(11)-enol, Obacunone, Beta-Sitosterol, Berberine, Sitosterol, Rutalidine, Fordimine, Ethanone, Gravacridoneshirlirine, and Goshuyamide I, with  $pIC_{50}$  values of 1.733, 1.491, 1.374, 1.374, .725, .470, .318 (Figure 4). Several studies have confirmed the therapeutic effects of some of these compounds in the treatment of liver cancer. Obacunone in mandarin (*Citrus reticulata* Blanco) has been shown in studies to inhibit a variety of human cancer cell lines, including leukemia (HL-60), ovarian cancer (SKOV-3), cervical cancer (Hela), gastric cancer (NCI-SNU-1), liver cancer (HepG2), and breast cancer (MCF-7). Obacunone had an  $IC_{50}$  of  $65.13 \pm 5.39 \mu\text{m}$  against HepG2 cells in an MTT assay (Tian et al., 2001). Mary (Ditty and Ezhilarasan, 2021) found that  $\beta$ -Sitosterol can increase cellular ROS levels, causing cell membrane damage and mitochondrial toxicity, as well as promoting HepG2 cell apoptosis. Berberine is an alkaloid that has been shown to inhibit the growth of various cancers. Ren et al. (2022) discovered that berberine inhibited hepatocarcinogenesis in mice by antagonizing the ATX-LPA-LPAR2-P38-leptin axis. Liu and Bai (2020) discovered that Sitosterol has effect on liver cancer with the help of analysis of network pharmacology. Ultimately, we screened out the top 10 compounds based on  $pIC_{50}$ , which may have better anti-liver cancer activity.

### 3.3 3D-QSAR model analysis

#### 3.3.1 Construction of the 3D-QSAR model by the HipHop method

We investigated the common chemical properties of the compounds and built a 3D-QSAR model by superimposing



the three-dimensional molecular structure. The HipHop method of the Discovery Studio software was used to generate nine 3D-QSAR pharmacophore models. Table 3 displays the pharmacophore model's matching parameters with the ten active compounds. According to the results, the 01 pharmacophore model had the highest rank score value of 57.220. The "HHA" shown in its "Feature" item indicates that it has two hydrophobic features and one hydrogen bond acceptor feature. The pharmacophore features in this model were directly matched to ten small molecules, and the Partial Hit revealed no partial matches to the pharmacophore for the ten small molecules. Furthermore, Max Hit indicated that three pharmacodynamic features could all be matched. The spatial distribution of Pharmacophore 01 is depicted in Figure 5. (Supplementary Figure S6 showed the spatial distribution of pharmacophore 02–09). As a result, we chose Pharmacophore 01 for further analysis and validation as the best constructed in this study.

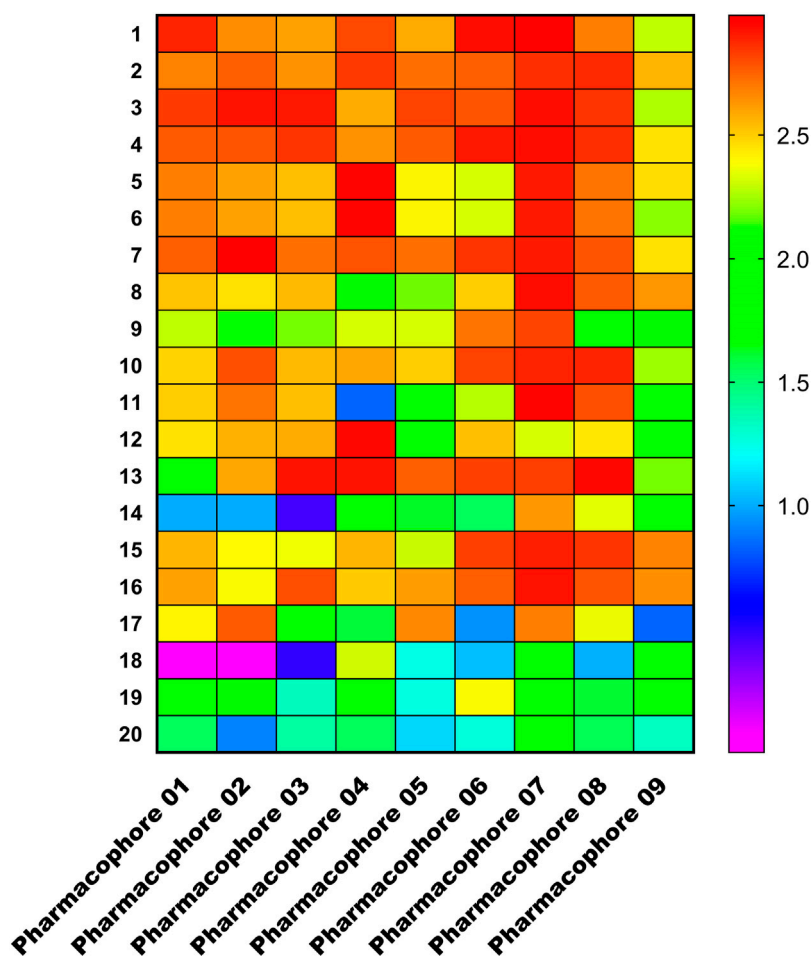


FIGURE 7  
Heat map of the training set compounds predicted by the nine pharmacophore models.

### 3.3.2 Construction of the 3D-QSAR model based on steric and electrostatic fields of small molecules

We built 3D-QSAR models based on the steric and electrostatic fields of the small molecules to investigate the non-covalent interactions in the structure of EF active compounds. Our 3D-QSAR model incorporates and visualizes the common important structural characteristics of a series of active compounds. The contour plots of the electrostatic field coefficients of the small molecules that match the 3D-QSAR models are shown in Figure 6A. In this system, the more negatively charged the substituents in the red region and the more positively charged the substituents in the blue region, the higher the activity of the compound. The contour plots of the steric field coefficients of small molecules that match the 3D-QSAR model are shown in Figure 6B. In this system, the yellow region indicates that increasing the volume of substituents is

detrimental to compound activity, whereas the blue region indicates that increasing the volume of substituents is beneficial to compound activity. The results showed that the electrostatic effects of the substituents, as well as the spatial distribution of the functional groups of the active compounds, affected their biological activities and may have contributed to the binding of key target proteins for liver cancer. Based on the force field information, this part of the study can help us screen and optimize the active compounds in EF.

### 3.3.3 Verification of 3D-QSAR pharmacophore model

We chose the top 20 training set compounds based on activity to verify that pharmacophores can correctly distinguish between active and inactive molecules. Figure 7 depicts a matching heatmap of the pharmacophore with the training set compounds, where the ordinate represents the



**TABLE 4 Matching results of nine pharmacophore models for compounds of the training set.**

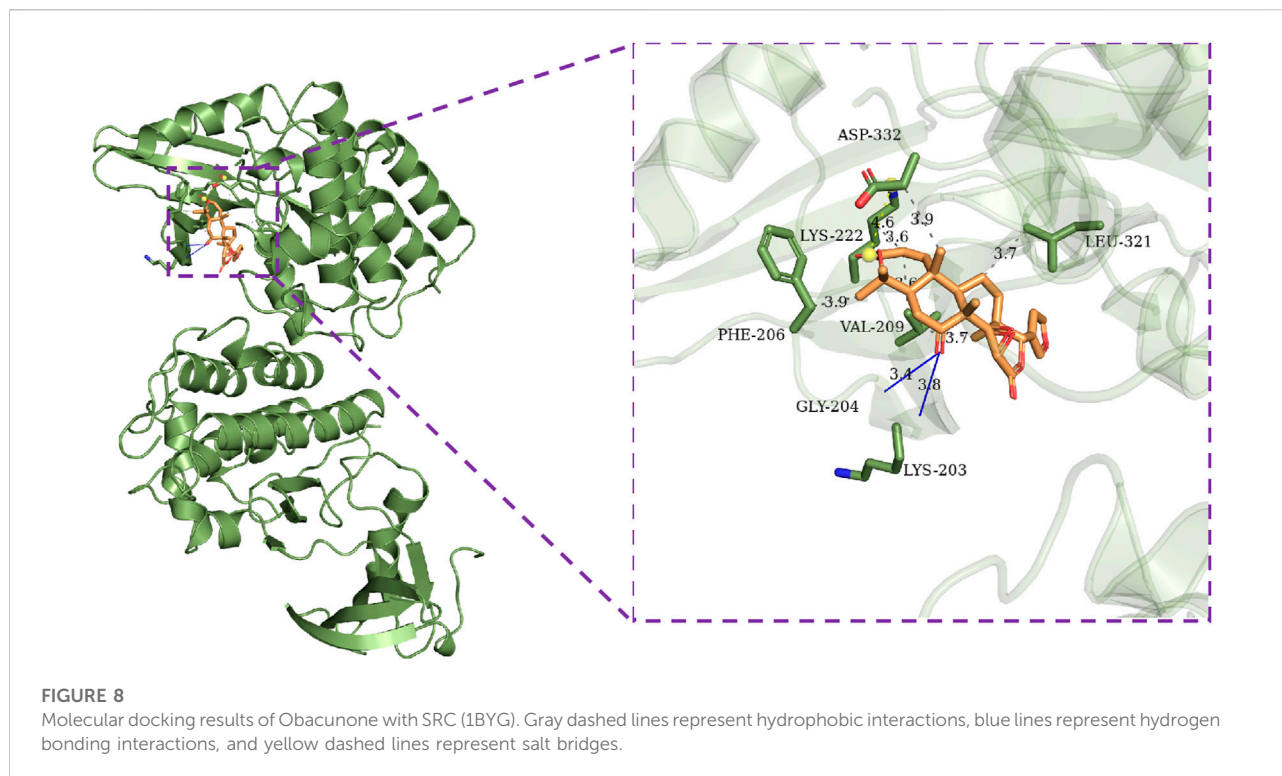
Compound no.	01	02	03	04	05	06	07	08	09
1	2.886	2.649	2.604	2.805	2.585	2.934	2.965	2.682	2.289
2	2.677	2.754	2.638	2.838	2.718	2.757	2.858	2.874	2.559
3	2.834	2.924	2.912	2.583	2.818	2.777	2.931	2.851	2.261
4	2.767	2.782	2.846	2.640	2.764	2.911	2.933	2.866	2.450
5	2.681	2.598	2.535	2.956	2.399	2.325	2.905	2.708	2.462
6	2.681	2.598	2.535	2.956	2.399	2.325	2.905	2.708	2.219
7	2.756	2.983	2.717	2.787	2.719	2.850	2.903	2.773	2.453
8	2.526	2.457	2.543	1.880	2.183	2.498	2.933	2.767	2.632
9	2.284	2.126	2.194	2.321	2.326	2.706	2.810	2.037	1.817
10	2.482	2.788	2.544	2.594	2.499	2.818	2.889	2.881	2.242
11	2.502	2.711	2.530	.836	2.035	2.271	2.949	2.790	1.660
12	2.444	2.568	2.582	2.942	1.874	2.529	2.328	2.435	1.996
13	2.034	2.593	2.919	2.919	2.755	2.824	2.827	2.938	2.192
14	1.000	1.000	.455	1.978	1.629	1.539	2.625	2.345	1.933
15	2.552	2.391	2.364	2.557	2.303	2.822	2.899	2.845	2.671
16	2.601	2.387	2.797	2.504	2.610	2.761	2.923	2.781	2.644
17	2.404	2.766	1.959	1.600	2.662	.935	2.684	2.358	.839
18	.000	.000	.485	2.307	1.239	1.046	1.929	1.008	2.048
19	1.806	1.810	1.338	1.971	1.254	2.380	1.868	1.605	2.003
20	1.533	.903	1.395	1.541	1.100	1.271	1.932	1.552	1.333

**TABLE 5 The affinity of compounds with SRC(1BYG) (kcal.mol<sup>-1</sup>).**

Active compound	Protein(PDBID)	Affinity
24-methyl-31-norlanost-9(11)-enol	SRC(1BYG)	-8.6
Obacunone	SRC(1BYG)	-9.4
beta-Sitosterol	SRC(1BYG)	-9.0
Sitosterol	SRC(1BYG)	-9.3
Fordimine	SRC(1BYG)	-7.8
Rutalinidine	SRC(1BYG)	-8.3
Berberine	SRC(1BYG)	-9.1
Ethanone	SRC(1BYG)	-6.6
Gravacridoneshlorine	SRC(1BYG)	-8.9
Goshuyamide_I	SRC(1BYG)	-8.7
Ponatinib	SRC(1BYG)	-9.8
Dasatinib	SRC(1BYG)	-8.7
STU	SRC(1BYG)	-10.9

20 training ensemble scores ranked in order of activity, the abscissa represents the pharmacophore 01–09, and the Fitvalue ranges from low to high, as indicated by the gradual purple to red color change. The darker the red color of each rectangular block in the figure, the greater the Fitvalue, thus the greater the corresponding compound activity. In theory, the active compounds in the training set should be red and orange, while the inactive compounds should be blue and purple, indicating that this pharmacophore can distinguish between active and inactive compounds. We discovered that the Fitvalue of the more active compound in pharmacophore 01 was higher than that of the less active compound, and that its fitvalue had a certain trend, indicating that pharmacophore 01 had ability to discriminate between active and inactive compounds. Pharmacophore 01 had the highest rank value.

Additionally, we used receiver operating characteristic (ROC) curve analysis to validate the pharmacophore (Al-Sha'er et al., 2022; Taha et al., 2014). ROC plots are a quantitative measure of whether a test can distinguish between two populations (typically active/inactive



compounds). It can be compared to other data sets. The area under the curve was used to evaluate test accuracy in ROC analysis (AUC). A test set of active and inactive compounds was used in our 3D-QSAR model to validate the pharmacophore model's selectivity. On the one hand, sensitivity is defined as the model's ability to identify positives, namely the extent to which an active molecule is distinguished from the inactive, or the proportion of the predicted active that is actually active:

$$\text{Sensitivity} = \text{TP} / (\text{TP} + \text{FN})$$

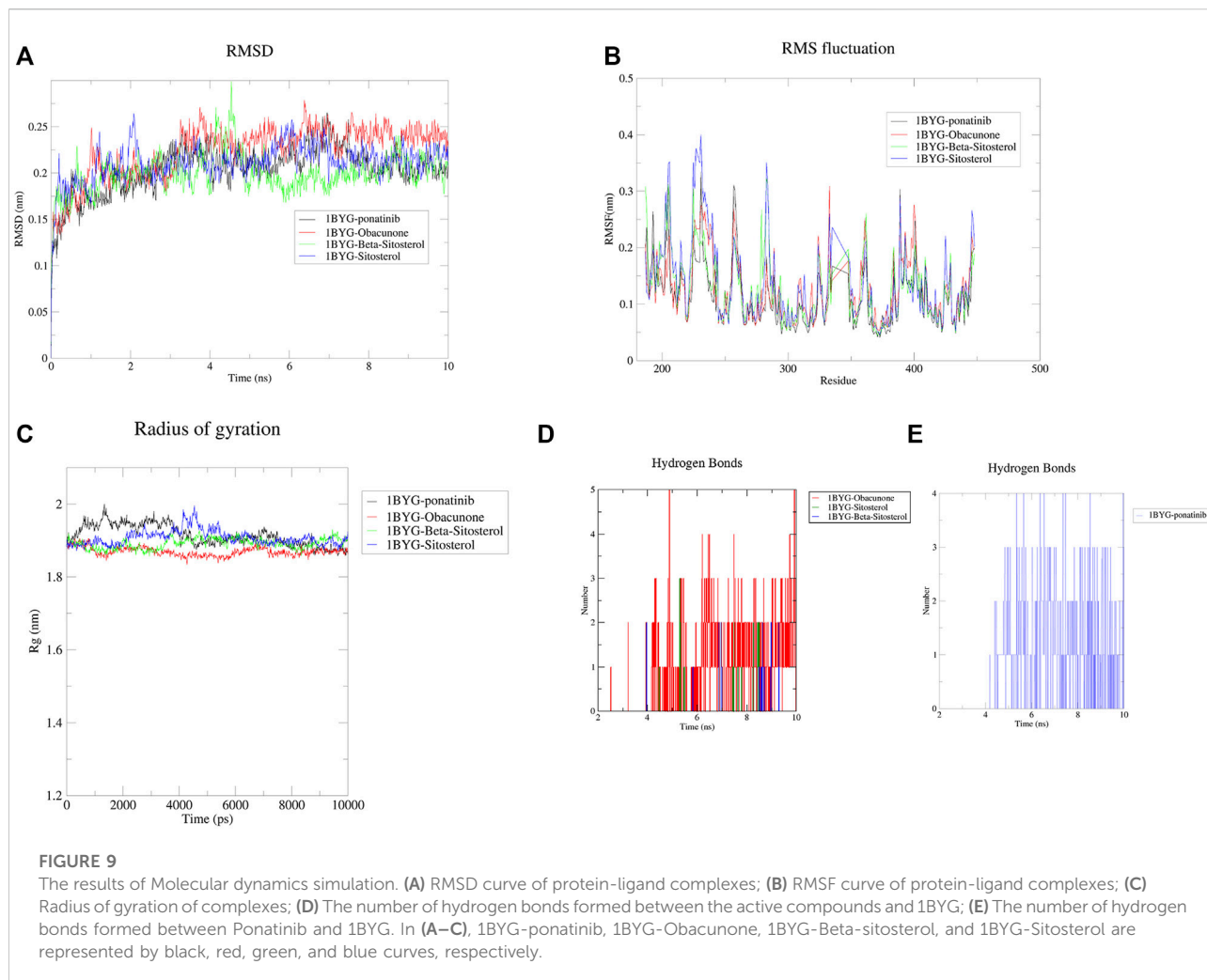
Specificity, on the other hand, is the ability of the model to determine negatives, or its discriminatory power for inactive compounds:

$$\text{Specific TN} / (\text{TN} + \text{FP})$$

ROC analysis results show that (Supplementary Figure S9; Supplementary Table S6), the ROC score of the pharmacophore 01 model is .768, and the sensitivity and specificity scores are both high. We believe pharmacophore 01 is the most effective pharmacophore hypothesis for distinguishing between active and inactive compounds. Therefore, we considered pharmacophore 01 was the best 3D-QSAR pharmacophore model. This means that pharmacophore model 01 may have anti-cancer effects on EF. The Fitvalue of the other pharmacophore models is shown in Table 4.

### 3.4 Molecular docking verification

This section of the study used molecular docking to validate the rationality of EF's 3D-QSAR pharmacophore model built from ten highly active compounds. The optimal conformation was chosen for each compound, and the RMSD of the conformations was less than 2. As shown in Table 5, the docking scores of the ten active compounds with SRC were all less than  $-7 \text{ kcal}\cdot\text{mol}^{-1}$ , with the exception of Ethanone. This implies that they play an important role in EF's anti-cancer process. Supplementary Figure S9 depicts their docking conditions. These compounds all bind to the amino acid residues of SRC *via* hydrophobic effects and hydrogen bonding interactions and have a similar docking mode. More specifically, Obacunone had the highest docking score with SRC, its antihepatoma activity *in vitro* has previously been reported, and its three-dimensional molecular docking state is shown in Figure 8. Obacunone primarily binds to SRC *via* hydrophobic and hydrogen bonding interactions. Obacunone could form hydrophobic interactions with amino acid residues PHE-206, VAL-209, THR-266, and PHE-333, with hydrophobic bond distances of 3.44, 2.61, 3.54, and 3.55 Å, respectively. Meanwhile, obacunone could form hydrogen bonding interactions with GLU-205 and PHE-206 at distances of 2.84 and 3.31 Å, respectively. Obacunone also has one salt bridge interaction with LYS-222. In addition, in order to improve the reliability of molecular docking, some reference drugs were used for docking, such as Ponatinib, Dasatinib, STU (Table 5). Their docking scores were  $-9.8$ ,  $-8.7$ , and  $-10.9 \text{ kcal}\cdot\text{mol}^{-1}$ ,



respectively. Some of the screened compounds have affinity values similar to the reference drugs, such as Obacunone, Beta-Sitosterol, Sitosterol, and Berberine. In general, these reference drugs interact with SRC *via* hydrophobic and hydrogen bond interactions. Hydrophobic interactions are formed by amino acid residues ILE-201, VAL-209, TYR-268, and LEU-321, and hydrogen bonds are formed by THR-266 and MET-269. Meanwhile, Ponatinib has some salt bridge interactions ([Supplementary Figure S10](#)). Overall, the screened compounds have similar docking modes to the reference drugs, and these docking interactions are consistent with the common features of pharmacophore 01.

### 3.5 MD simulations

After a 10 ns molecular dynamics simulation, we could further examine how the screened compounds interacted with the protein SRC (1BYG). Obacunone, Beta-sitosterol, and sitosterol were chosen for MD simulation analysis in this work because they

had superior docking scores (less than  $-9 \text{ kcal.mol}^{-1}$ ) than other compounds. [Figure 9A](#) shows that throughout the entire procedure, the RMSD of 1BYG Obacunone, 1BYG Beta sitosterol, and 1BYG Sitosterol maintained between .1 and .3, and the fluctuation became stable after 10 ns. It indicates that the 10 ns trajectory conformation of compounds does not reveal substantial structural differences from ponatinib, implying that the ligand and complex structures are stable.

The root mean square fluctuation (RMSF) curve was used to investigate the local changes in protein chain residues. In the 10 ns trajectory files, the fluctuation profiles of the amino acid residues of the complexes (1BYG-Obacunone, 1BYG-Beta-sitosterol, and 1BYG-Sitosterol) were visualized in [Figure 9B](#). RMSF value is lower than 0.4 nm, and a stable fluctuation is generated at about .15, which provides an appropriate basis for subsequent research. 1BYG-obacunone fluctuated surprisingly little in these compounds until about the 300th residue, when it peaked at .3 nm. 1BYG-Beta-sitosterol and 1BYG-Sitosterol have peaks at .32 and .4 nm, respectively with substantial variations in

position before residue 300. Their fluctuation trajectories followed the same pattern as 1BYG-Ponatinib.

The radius of gyration (Rg) is a measure of a complex system's stability in terms of the structural compactness of the molecular dynamics trajectory (Shahbaaz et al., 2019). Rg can also be used to confirm the complex's stable folding during the simulation. If Rg values are relatively consistent throughout the simulation, the protein structure is considered stable (Ghasemi et al., 2016). A higher Rg value indicates that the protein is more labile, while a lower value indicates that the protein is more stable. In Figure 9C, Rg values of 1BYG-Obacunone were lower and more stable than those of others, this leads in less structural bias and higher stability in the obacunone complexes during simulations.

In addition, we analyzed the number of hydrogen bonds for trajectories lasting 10 ns. Figure 9D shows the hydrogen bonding interaction of obacunone, beta-sitosterol and sitosterol at a distance of 3.5 Å (.35 nm). The maximum number of hydrogen bonds found for obacunone, beta-sitosterol, and sitosterol were 5, 2, and 3, respectively. Over the course of 10 ns, beta-sitosterol, and sitosterol formed fewer hydrogen bonds with 1BYG, indicating poor binding stability. Obacunone formed five hydrogen bonds with 1BYG between 5 and 10 ns, and the number of hydrogen bonds formed was the greatest throughout the simulation process, ensuring better stability. Furthermore, obacunone has a similar density of hydrogen bonding conditions to ponatinib (Figure 9E), which explains its superior binding activity.

## 4 Conclusion

In this study, some potential active compounds such as Obacunone, Beta-sitosterol, Sitosterol, and others were screened using network pharmacology, and SRC was clearly identified as the most promising target of EF in the treatment of liver cancer. The top three signaling pathways are the EGFR signaling pathway, the ErbB signaling pathway, PD-L1 expression, and the PD-1 checkpoint pathway. In addition, the 2-dimensional QSAR pharmacophore model identified 24-methyl-31-norlanost-9(11)-enol, Obacunone, Beta-sitosterol, Sitosterol, Fordimine, Rutalinidine, Berberine, Ethanone, Gravacridoneshlorine, and Goshuyamide I as highly active compounds. The 3D-QSAR model we created revealed that Pharmacophore 01 had two hydrophobic features and one hydrogen bond acceptor feature. Heatmap and ROC analysis results revealed that pharmacophore 01 possessed high selectivity as well as the ability to distinguish between active and inactive compounds. The molecular docking results confirmed the active compounds' stable binding to SRC. Furthermore, MD simulations demonstrated the stability of Obacunone, Beta-sitosterol, and Sitosterol in dynamic systems and highlighted Obacunone's prominent binding capacity. The pharmacophore

model proposed in this study provides theoretical support for further screening of effective Chinese medicine compounds against liver cancer and compound structural optimization. Meanwhile, for the optimal compounds, additional pharmacodynamic and pharmacological studies will be conducted to clarify their mechanism of action for the treatment of liver cancer.

## Data availability statement

The datasets presented in this study can be found in online repositories. The names of the repository/repositories and accession number(s) can be found in the article/Supplementary Material.

## Author contributions

P-YC: Select topic, research proposal design, data analysis, and paper writing. L-TH: Syntax optimization, review, and editing.

## Funding

This work was supported by the Funds for Key Program for Traditional Chinese Medicine of Hubei University of Chinese Medicine (2022ZZXZ004).

## Conflict of interest

The authors declare that the research was conducted in the absence of any commercial or financial relationships that could be construed as a potential conflict of interest.

## Publisher's note

All claims expressed in this article are solely those of the authors and do not necessarily represent those of their affiliated organizations, or those of the publisher, the editors and the reviewers. Any product that may be evaluated in this article, or claim that may be made by its manufacturer, is not guaranteed or endorsed by the publisher.

## Supplementary material

The Supplementary Material for this article can be found online at: <https://www.frontiersin.org/articles/10.3389/fchem.2022.1060500/full#supplementary-material>



## References

- Adelusi, T. I., Abdul-Hammed, M., Idris, M. O., Oyedele, Q. K., and Adedotun, I. O. (2021). Molecular dynamics, quantum mechanics and docking studies of some Keap1 inhibitors - an insight into the atomistic mechanisms of their antioxidant potential. *Heliyon* 7 (6), e07317. doi:10.1016/j.heliyon.2021.e07317
- Ahmed, N., Anwar, S., and Thet Htar, T. (2017). Docking based 3D-QSAR study of tricyclic guanidine analogues of batzelladine K as anti-malarial agents. *Front. Chem.* 5, 36. doi:10.3389/fchem.2017.00036
- Al-Sha'er, M. A., Basheer, H. A., and Taha, M. O. (2022). Discovery of new PKN2 inhibitory chemotypes via QSAR-guided selection of docking-based pharmacophores. *Mol. Divers.* doi:10.1007/s11030-022-10434-410.1007/s11030-022-10434-4
- Anwanwan, D., Singh, S. K., Singh, S., Saikam, V., and Singh, R. (2020). Challenges in liver cancer and possible treatment approaches. *Biochim. Biophys. Acta Rev. Cancer* 1873 (1), 188314. doi:10.1016/j.bbcan.2019.188314
- Bain, J., Plater, L., Elliott, M., Shpiro, N., Hastie, C. J., McLauchlan, H., et al. (2007). The selectivity of protein kinase inhibitors: A further update. *Biochem. J.* 408 (3), 297–315. doi:10.1042/bj20070797
- Cao, W., Chen, H. D., Yu, Y. W., Li, N., and Chen, W. Q. (2021). Changing profiles of cancer burden worldwide and in China: A secondary analysis of the global cancer statistics 2020. *Chin. Med. J. Engl.* 134 (7), 783–791. doi:10.1097/cm9.0000000000001474
- Ceppi, P., Rapa, I., Lo Iacono, M., Righi, L., Giorcelli, J., Pautasso, M., et al. (2012). Expression and pharmacological inhibition of thymidylate synthase and Src kinase in nonsmall cell lung cancer. *Int. J. Cancer* 130 (8), 1777–1786. doi:10.1002/ijc.26188
- Chen, P. Y., Yuan, C., Hong, Z. C., Zhang, Y., Ke, X. G., Yu, B., et al. (2021). Revealing the mechanism of "Huai Hua San" in the treatment of ulcerative colitis based on network pharmacology and experimental study. *J. Ethnopharmacol.* 281, 114321. doi:10.1016/j.jep.2021.114321
- Chen, Y., Chen, X., Ding, X., and Wang, Y. (2019). Afatinib, an EGFR inhibitor, decreases EMT and tumorigenesis of Huh-7 cells by regulating the ERK-VEGF/MMP9 signaling pathway. *Mol. Med. Rep.* 20 (4), 3317–3325. doi:10.3892/mmr.2019.10562
- Chin, C. H., Chen, S. H., Wu, H. H., Ho, C. W., Ko, M. T., and Lin, C. Y. (2014). cytoHubba: identifying hub objects and sub-networks from complex interactome. *BMC Syst. Biol.* 8 (4), S11. doi:10.1186/1752-0509-8-s4-s11
- Cho, J. H., Lee, R. H., Jeon, Y. J., Shin, J. C., Park, S. M., Choi, N. J., et al. (2015). Role of transcription factor Sp1 in the 4-O-methylhonokiol-mediated apoptotic effect on oral squamous cancer cells and xenograft. *Int. J. Biochem. Cell Biol.* 64, 287–297. doi:10.1016/j.biocel.2015.05.007
- Ditty, M. J., and Ezhilarasan, D. (2021).  $\beta$ -sitosterol induces reactive oxygen species-mediated apoptosis in human hepatocellular carcinoma cell line. *Avicenna J. Phytomed* 11 (6), 541–550. doi:10.22038/ajp.2021.17746
- Dong, L., Shi, H., Ji, G., and Wu, D. (2010). Effects of *Coptis chinensis* and *Evodia rutaecarpa* water extract on DMH-induced precancerous lesion of colon. *Zhongguo Zhong Yao Za Zhi* 35 (9), 1185–1188. doi:10.4268/cjcm20100923
- Dumaual, C. M., Sandusky, G. E., Soo, H. W., Werner, S. R., Crowell, P. L., and Randall, S. K. (2012). Tissue-specific alterations of PRL-1 and PRL-2 expression in cancer. *Am. J. Transl. Res.* 4 (1), 83–101.
- Dwivedi, N., Mishra, B. N., and Katoch, V. M. (2011). 2D-QSAR model development and analysis on variant groups of anti-tuberculosis drugs. *Bioinformation* 7 (2), 82–90. doi:10.6026/97320630007082
- El-Serag, H. B., Marrero, J. A., Rudolph, L., and Reddy, K. R. (2008). Diagnosis and treatment of hepatocellular carcinoma. *Gastroenterology* 134 (6), 1752–1763. doi:10.1053/j.gastro.2008.02.090
- Elekofehinti, O. O., Iwaloye, O., Molehin, O. R., and Famusiwa, C. D. (2021). Identification of lead compounds from large natural product library targeting 3C-like protease of SARS-CoV-2 using E-pharmacophore modelling, QSAR and molecular dynamics simulation. *Silico Pharmacol.* 9 (1), 49. doi:10.1007/s40203-021-00109-7
- Fathi, M. A. A., Abd El-Hafeez, A. A., Abdelhamid, D., Abbas, S. H., Montano, M. M., and Abdel-Aziz, M. (2019). 1, 3, 4-oxadiazole/chalcone hybrids: Design, synthesis, and inhibition of leukemia cell growth and EGFR, Src, IL-6 and STAT3 activities. *Bioorg Chem.* 84, 150–163. doi:10.1016/j.bioorg.2018.11.032
- Ferreira, L. G., Dos Santos, R. N., Oliva, G., and Andricopulo, A. D. (2015). Molecular docking and structure-based drug design strategies. *Molecules* 20 (7), 13384–13421. doi:10.3390/molecules200713384
- Ghasemi, F., Zomorodipour, A., Karkhane, A. A., and Khorramzadeh, M. R. (2016). *In silico* designing of hyper-glycosylated analogs for the human coagulation factor IX. *J. Mol. Graph Model* 68, 39–47. doi:10.1016/j.jmgm.2016.05.011
- Hajalsiddiq, T. T. H., Osman, A. B. M., and Saeed, A. E. M. (2020). 2D-QSAR modeling and molecular docking studies on 1H-Pyrazole-1-carbothioamide derivatives as EGFR kinase inhibitors. *ACS Omega* 5 (30), 18662–18674. doi:10.1021/acsomega.0c01323
- He, W. Q., Gao, X., Gao, L., Ma, Y., Sun, D., and Sun, J. (2021). Contrasting trends of primary liver cancer mortality in Chinese mongol and non-mongol. *Asian Pac J. Cancer Prev.* 22 (9), 2757–2763. doi:10.31557/apjcp.2021.22.9.2757
- Hiscox, S., and Nicholson, R. I. (2008). Src inhibitors in breast cancer therapy. *Expert Opin. Ther. Targets* 12 (6), 757–767. doi:10.1517/14728222.12.6.757
- Hu, C. Y., Wu, H. T., Su, Y. C., Lin, C. H., Chang, C. J., and Wu, C. L. (2017). Evodiamine exerts an anti-hepatocellular carcinoma activity through a WWOX-dependent pathway. *Molecules* 22 (7), 1175. doi:10.3390/molecules22071175
- Huang, S. Y., and Zou, X. (2010). Advances and challenges in protein-ligand docking. *Int. J. Mol. Sci.* 11 (8), 3016–3034. doi:10.3390/ijms11083016
- Imran, S., Taha, M., Ismail, N. H., Kashif, S. M., Rahim, F., Jamil, W., et al. (2015). Synthesis of novel flavone hydrazones: *In-vitro* evaluation of  $\alpha$ -glucosidase inhibition, QSAR analysis and docking studies. *Eur. J. Med. Chem.* 105, 156–170. doi:10.1016/j.ejmech.2015.10.017
- Jiang, L., He, Y., Luo, G., Yang, Y., Li, G., and Zhang, Y. (2016). Discovery of potential novel microsomal triglyceride transfer protein inhibitors via virtual screening of pharmacophore modelling and molecular docking. *Mol. Simul.* 42, 1223–1232. doi:10.1080/08927022.2016.1149701
- Jin, Q., Cheng, M., Xia, X., Han, Y., Zhang, J., Cao, P., et al. (2021). Down-regulation of MYH10 driven by chromosome 17p13.1 deletion promotes hepatocellular carcinoma metastasis through activation of the EGFR pathway. *J. Cell Mol. Med.* 25 (24), 11142–11156. doi:10.1111/jcmm.17036
- Kassebaum, N. J., Bertozzi-Villa, A., Coggeshall, M. S., Shackelford, K. A., Steiner, C., Heuton, K. R., et al. (2014). Global, regional, and national levels and causes of maternal mortality during 1990–2013: A systematic analysis for the global burden of disease study 2013. *Lancet* 384 (9947), 980–1004. doi:10.1016/s0140-6736(14)60696-6
- Li, B., Yin, X., Cen, B., Duan, W., Lin, G., Wang, X., et al. (2022). High value-added application of natural forest product  $\alpha$ -pinene: Design, synthesis and 3D-QSAR study of novel  $\alpha$ -campholenic aldehyde-based 4-methyl-1, 2, 4-triazole-thioether compounds with significant herbicidal activity. *Nat. Prod. Res.* 1–6. doi:10.1080/14786419.2022.211717610.1080/14786419.2022.2117176
- Li, M., and Wang, C. (2020). Traditional uses, phytochemistry, pharmacology, pharmacokinetics and toxicology of the fruit of tetradium rutiarpum: A review. *J. Ethnopharmacol.* 263, 113231. doi:10.1016/j.jep.2020.113231
- Liao, W. Q., Li, B., Li, L., and Zhao, J. N. (2014). Study on molecular mechanism of *Euodiae Fructus* on liver toxicity in MICE. *Zhongguo Zhong Yao Za Zhi* 39 (24), 1–17.
- Liu, B., and Bai, C. (2020). Regulatory mechanisms of coicis semen on bionetwork of liver cancer based on network pharmacology. *Biomed. Res. Int.* 2020, 1. doi:10.1155/2020/5860704
- Luo, X., Zheng, E., Wei, L., Zeng, H., Qin, H., Zhang, X., et al. (2021). The fatty acid receptor CD36 promotes HCC progression through activating Src/PI3K/AKT axis-dependent aerobic glycolysis. *Cell Death Dis.* 12 (4), 328. doi:10.1038/s41419-021-03596-w
- Ma, X., Qiu, Y., Zhu, L., Zhao, Y., Lin, Y., Ma, D., et al. (2020). NOD1 inhibits proliferation and enhances response to chemotherapy via suppressing SRC-MAPK pathway in hepatocellular carcinoma. *J. Mol. Med. Berl.* 98 (2), 221–232. doi:10.1007/s00109-019-01868-9
- Martin, M. W., Newcomb, J., Nunes, J. J., McGowan, D. C., Armistead, D. M., Boucher, C., et al. (2006). Novel 2-aminopyrimidine carbamates as potent and orally active inhibitors of lck: Synthesis, SAR, and *in vivo* antiinflammatory activity. *J. Med. Chem.* 49 (16), 4981–4991. doi:10.1021/jm060435i
- Meng, X. Y., Zhang, H. X., Mezei, M., and Cui, M. (2011). Molecular docking: A powerful approach for structure-based drug discovery. *Curr. Comput. Aided Drug Des.* 7 (2), 146–157. doi:10.2174/157340911795677602
- Meng, Y., Zhao, Q., An, L., Jiao, S., Li, R., Sang, Y., et al. (2021). A TNFR2-hnRNPK Axis promotes primary liver cancer development via activation of YAP signaling in hepatic progenitor cells. *Cancer Res.* 81 (11), 3036–3050. doi:10.1158/0008-5472.Can-20-3175
- Miethe, C., Torres, L., Zamora, M., and Price, R. S. (2021). Inhibition of PI3K/Akt and ERK signaling decreases visfatin-induced invasion in liver cancer cells. *Horm. Mol. Biol. Clin. Investig.* 42 (4), 357–366. doi:10.1515/hmbci-2021-0011
- Mo, C. F., Li, J., Yang, S. X., Guo, H. J., Liu, Y., Luo, X. Y., et al. (2020). IQGAP1 promotes anoikis resistance and metastasis through Rac1-dependent ROS accumulation and activation of Src/FAK signalling in hepatocellular carcinoma. *Br. J. Cancer* 123 (7), 1154–1163. doi:10.1038/s41416-020-0970-z

- Muratov, E. N., Bajorath, J., Sheridan, R. P., Tetko, I. V., Filimonov, D., Poroikov, V., et al. (2020). QSAR without borders. *Chem. Soc. Rev.* 49 (11), 3525–3564. doi:10.1039/d0cs00098a
- Ni, Q., Chen, Z., Zheng, Q., Xie, D., Li, J. J., Cheng, S., et al. (2020). Epithelial V-like antigen 1 promotes hepatocellular carcinoma growth and metastasis via the ERBB-PI3K-AKT pathway. *Cancer Sci.* 111 (5), 1500–1513. doi:10.1111/cas.14331
- O'Reilly, M., Cleasby, A., Davies, T. G., Hall, R. J., Ludlow, R. F., Murray, C. W., et al. (2019). Crystallographic screening using ultra-low-molecular-weight ligands to guide drug design. *Drug Discov. Today* 24 (5), 1081–1086. doi:10.1016/j.drudis.2019.03.009
- Park, S. Y., Park, C., Park, S. H., Hong, S. H., Kim, G. Y., Hong, S. H., et al. (2017). Induction of apoptosis by ethanol extract of *Evodia rutaecarpa* in HeLa human cervical cancer cells via activation of AMP-activated protein kinase. *Biosci. Trends* 10 (6), 467–476. doi:10.5582/bst.2016.01170
- Rampogu, S., Son, M., Baek, A., Park, C., Rana, R. M., Zeb, A., et al. (2018). Targeting natural compounds against HER2 kinase domain as potential anticancer drugs applying pharmacophore based molecular modelling approaches. *Comput. Biol. Chem.* 74, 327–338. doi:10.1016/j.compbiolchem.2018.04.002
- Ren, G., Guo, J. H., Feng, C. L., Ding, Y. W., Dong, B., Han, Y. X., et al. (2022). Berberine inhibits carcinogenesis through antagonizing the ATX-LPA-LPAR2-p38-leptin axis in a mouse hepatoma model. *Mol. Ther. Oncolytics* 26, 372–386. doi:10.1016/j.omto.2022.08.001
- Ren, Z., and Schaefer, T. S. (2002). ErbB-2 activates Stat3 alpha in a Src- and JAK2-dependent manner. *J. Biol. Chem.* 277 (41), 38486–38493. doi:10.1074/jbc.M112438200
- Roskoski, R., Jr. (2015). Src protein-tyrosine kinase structure, mechanism, and small molecule inhibitors. *Pharmacol. Res.* 94, 9–25. doi:10.1016/j.phrs.2015.01.003
- Schenone, S., Manetti, F., and Botta, M. (2007). SRC inhibitors and angiogenesis. *Curr. Pharm. Des.* 13 (21), 2118–2128. doi:10.2174/138161207781039580
- Shahbaaz, M., Nkaule, A., and Christoffels, A. (2019). Designing novel possible kinase inhibitor derivatives as therapeutics against *Mycobacterium tuberculosis*: An *in silico* study. *Sci. Rep.* 9 (1), 4405. doi:10.1038/s41598-019-40621-7
- Shan, Q. Y., Sang, X. N., Hui, H., Shou, Q. Y., Fu, H. Y., Hao, M., et al. (2020). Processing and polyherbal formulation of tetradium rutiarpum (A. Juss.) hartley: Phytochemistry, pharmacokinetics, and toxicity. *Front. Pharmacol.* 11, 133. doi:10.3389/fphar.2020.00133
- Shang, N., Wang, H., Bank, T., Perera, A., Joyce, C., Kuffel, G., et al. (2019). Focal adhesion kinase and  $\beta$ -catenin cooperate to induce hepatocellular carcinoma. *Hepatology* 70 (5), 1631–1645. doi:10.1002/hep.30707
- Sherman, B. T., Hao, M., Qiu, J., Jiao, X., Baseler, M. W., Lane, H. C., et al. (2022). David: A web server for functional enrichment analysis and functional annotation of gene lists (2021 update). *Nucleic Acids Res.* 50 (W1), W216–W221. doi:10.1093/nar/gkac194
- Sia, D., Villanueva, A., Friedman, S. L., and Llovet, J. M. (2017). Liver cancer cell of origin, molecular class, and effects on patient prognosis. *Gastroenterology* 152 (4), 745–761. doi:10.1053/j.gastro.2016.11.048
- Taha, M. O., Al-Sha'er, M. A., Khanfar, M. A., and Al-Nadaf, A. H. (2014). Discovery of nanomolar phosphoinositide 3-kinase gamma (PI3K $\gamma$ ) inhibitors using ligand-based modeling and virtual screening followed by *in vitro* analysis. *Eur. J. Med. Chem.* 84, 454–465. doi:10.1016/j.ejmech.2014.07.056
- Tian, Q., Miller, E. G., Ahmad, H., Tang, L., and Patil, B. S. (2001). Differential inhibition of human cancer cell proliferation by citrus limonoids. *Nutr. Cancer* 40 (2), 180–184. doi:10.1207/s15327914nc402\_15
- Tong, Z., Li, M., Wang, W., Mo, P., Yu, L., Liu, K., et al. (2015). Steroid receptor coactivator 1 promotes human hepatocellular carcinoma progression by enhancing wnt/ $\beta$ -catenin signaling. *J. Biol. Chem.* 290 (30), 18596–18608. doi:10.1074/jbc.M115.640490
- Verma, J., Khedkar, V. M., and Coutinho, E. C. (2010). 3D-QSAR in drug design--a review. *Curr. Top. Med. Chem.* 10 (1), 95–115. doi:10.2174/156802610790232260
- Wang, H., Wang, X., Li, X., Zhang, Y., Dai, Y., Guo, C., et al. (2012). QSAR study and the hydrolysis activity prediction of three alkaline lipases from different lipase-producing microorganisms. *Lipids Health Dis.* 11, 124. doi:10.1186/1476-511x-11-124
- Wang, H. Y., Cao, Z. X., Li, L. L., Jiang, P. D., Zhao, Y. L., Luo, S. D., et al. (2008). Pharmacophore modeling and virtual screening for designing potential PLK1 inhibitors. *Bioorg. Med. Chem. Lett.* 18 (18), 4972–4977. doi:10.1016/j.bmcl.2008.08.033
- Xia, Z., and Tang, Z. (2021). Network pharmacology analysis and experimental pharmacology study explore the mechanism of gambogic acid against endometrial cancer. *ACS Omega* 6 (16), 10944–10952. doi:10.1021/acso.1c00696
- Yang, F., Shi, L., Liang, T., Ji, L., Zhang, G., Shen, Y., et al. (2017). Anti-tumor effect of evodiamine by inducing Akt-mediated apoptosis in hepatocellular carcinoma. *Biochem. Biophys. Res. Commun.* 485 (1), 54–61. doi:10.1016/j.bbrc.2017.02.017
- Yang, J., Zhang, X., Liu, L., Yang, X., Qian, Q., and Du, B. (2021). c-Src promotes the growth and tumorigenesis of hepatocellular carcinoma via the Hippo signaling pathway. *Life Sci.* 264, 118711. doi:10.1016/j.lfs.2020.118711
- Yoon, J. Y., Jeong, H. Y., Kim, S. H., Kim, H. G., Nam, G., Kim, J. P., et al. (2013). Methanol extract of *Evodia lepta* displays Syk/Src-targeted anti-inflammatory activity. *J. Ethnopharmacol.* 148 (3), 999–1007. doi:10.1016/j.jep.2013.05.030
- You, H., Meng, K., and Wang, Z. Y. (2018). The ER- $\alpha$ 36/EGFR signaling loop promotes growth of hepatocellular carcinoma cells. *Steroids* 134, 78–87. doi:10.1016/j.steroids.2018.02.007
- Zhao, P. W., Zhang, J. W., Liu, Y., Liu, Y., Liu, J. W., and Huang, J. Z. (2020). SRC-1 and Twist1 are prognostic indicators of liver cancer and are associated with cell viability, invasion, migration and epithelial-mesenchymal transformation of hepatocellular carcinoma cells. *Transl. Cancer Res.* 9 (2), 603–612. doi:10.21037/tcr.2019.11.56
- Zhao, Z., He, X., Han, W., Chen, X., Liu, P., Zhao, X., et al. (2019). Genus tetradium L.: A comprehensive review on traditional uses, phytochemistry, and pharmacological activities. *J. Ethnopharmacol.* 231, 337–354. doi:10.1016/j.jep.2018.11.035